Constructive heterogeneous object modeling using signed approximate real distance functions

Pierre-Alain Fayolle, Alexander Pasko, Benjamin Schmitt, Nikolay Mirenkov

The University of Aizu, Department of Information Systems
Hosei University
Computer Graphics Research Institute and Hosei University, Digital Media Professional
The University of Aizu, Department of Information Systems

ABSTRACT

We introduce a smooth approximation of the *min* / *max* operations, called SARDF (Signed Approximate Real Distance Function), for maintaining an approximate signed distance function in constructive shape modeling. We apply constructive distance-based shape modeling to design objects with heterogeneous material distribution in the constructive hypervolume model framework. The introduced distance approximation helps intuitively model material distributions parameterized by distances to so-called material features. The smoothness of the material functions, provided here by the smoothness of the defining function for the shape, helps to avoid undesirable singularities in the material distribution, like stress or concentrations. We illustrate application of the SARDF operations by two- and three-dimensional heterogeneous object modeling case studies.

Keywords

Constructive heterogeneous object modeling, distance function approximation, set-theoretic operations, Function Representation (FRep).

1 INTRODUCTION

Solid modeling methods have mostly focused so far on developing models that capture only the geometry of objects, under the assumption that most of them are homogeneous. Recently, a particular attention has been paid to heterogeneous objects modeling, where an object has a number of non-uniformly distributed attributes assigned at each point and varying in space. These attributes may or may not be continuous and have different nature such as photometric characteristics, material density or distribution, physical properties, and others. Heterogeneous objects are widely used in different areas of design and engineering such as rapid prototyping, physical simulations, geological and medical modeling.

We provide in this work new functional definitions for the set-theoretic operations to be used in constructive distance-based modeling of heterogeneous objects. These functions provide a smooth controlled approximation of *min* / *max* used traditionally in constructive modeling of distance fields ([1,2]). In the present work, we try to propose an answer to the question on how can one practically construct heterogeneous objects where the material distributions are parameterized by the distance to material features.

1.1 Previous works

1.1.1 Heterogeneous modeling

Several techniques for modeling heterogeneous objects are already available, presenting some noticeable analogies with homogeneous object modeling. Existing homogeneous object models include surface representations (boundary representation, feature based models); and volumetric representations (voxel arrays, adaptive spatial decompositions, Function Representation, etc). Each homogeneous model has been extended to allow for the underlying model to handle heterogeneity.

R-sets are considered as a basis for modeling and are extended for material inclusion in [3]. An object is subdivided in components; each of them is homogeneous inside and has an assigned material index. Set-theoretic operations can be applied to the solid's components with the corresponding operations on the material. Unfortunately, this modeling technique is limited to the representation of discretely varying material properties. In [4], a more general model is proposed: the geometry is represented by the point set decomposition into a finite set of closed 3-cells, whereas the attributes are defined by a collection of functions, which map the object geometry to several attributes. Such a mathematical model is known as a fiber bundle, with the geometrical model playing the role of the base space. Several other works are using the same model, extending it in various directions ([5,6]). However, as noticed in [7], this model does not really offer concrete computational solutions.

Volumetric representations naturally define solids: a homogeneous object can be defined as a subset of the 3D space, with an additional scalar value given at any point. In the case of a spatial enumeration, like voxels [8], extension to heterogeneity consists in adding a scalar

value for each attribute [9]. The drawback of this method is the difficulty to directly describe the material distribution, without using a data acquisition device (therefore it is supposed that the object to be modeled already exists). Furthermore, the discrete property of the model requires some special approximation procedures.

In [10], a general mathematical framework for modeling heterogeneous objects is proposed. An object is defined as a multidimensional point-set in space; its geometry is characterized by a signed real function at least continuous [11]; different attributes are also defined by functions and their domains of definition. In this framework, the domain of definition of an attribute is called a *space partition*. Both the geometry and the space partitions of the object can be defined by constructive modeling, using either the general R-functions [12], or *min* / *max* functions [1,2]. However, the problem of parameterization and control of attributes in the case of material modeling is left unanswered.

A continuous volumetric representation was proposed in [13], where a B-spline volume is used to model the object geometry, whereas the attributes are modeled by means of diffusion. This model seems to suffer from the lack of flexibility of the geometry limited to volume splines.

Biswas et al. [7] are interested in the representation and control of material distributions by some intuitive parameters related to the geometry of the solid and/or its material features for meshfree modeling. They propose to use the distance functions from material features (point-sets of any dimension with known material properties) as these parameters. It appears from the existing literature that the (Euclidean) distance, or functions of the distance function are indeed the most common types of material functions constructed by methods based on spatial discretization [14,15,16]. The authors of [7] demonstrate that this approach is theoretically complete as it can represent all material functions. However, in their work the modeling of the solid geometry and the material features by Euclidean distance fields is practically not considered.

1.1.2 Signed distance function construction

The Euclidean distance field (or Euclidean distance function) for a given point-set S in the Euclidean space E^n, is a mapping that associates with each point of E^n a real value corresponding to the shortest distance between the given point and every other point in S. Distance fields already have numerous applications in geometric modeling [17], shape metamorphosis [18], object reconstruction from cross-sections [19], robust rendering with sphere tracing [20], generation of skeletal shape representation [21], and other areas. However, it should be noticed that the term distance is often used for different types of distance functions (algebraic, Euclidean, or others) without precise specification. A comparison between Euclidean and algebraic distances to quadric surfaces [22] suggests that the Euclidean one is preferable. In the remainder of the paper, the term distance always refers to the Euclidean distance, unless explicitly specified.

The signed distance function describing a solid is defined as the Euclidean distance from the current point to the surface of the solid, with a sign indicating whether the point is inside or outside the solid [23]. The construction of the signed Euclidean distance function or at least its approximation for the given shape is rather problematic. Deriving an analytical expression is a tedious or sometimes even impossible work. Interpolation methods can be used to provide numerical evaluation at any point of the signed distance function. Given a solid S, the distance to S (its surface) can be sampled on a spatial grid (see [24,25] and references therein) and then interpolated using some basis functions (see [26] and references therein).

Level-set methods [27] can be used to reconstruct an implicit surface (as the zero iso-level of an approximated signed distance function) from unorganized point-sets [28]. However as noticed by Ohtake et al [29] the method is expensive in time and memory. Though the solution is an implicit surface, defined by a signed distance function, its values are known only at the grid nodes and correspond to the solution of a partial derivative equation given by numerical procedures.

Both level-set methods and interpolation may suffer from numerical issues and a loss of accuracy depending on factors such as the choice of the basis, the sampling of the discrete distance field, or the quality of the input data. Finally, both of these methods rely either on: the existence of a discrete distance field (the values of the distance function are known on a finite number of nodes on a grid) or the construction of this discrete distance field from a set of discrete points (and normals) on the surface of the shape (see [24,25] and references therein). As a consequence, both of these methods require that the object already exists (either as a computer model or physically and ready to be scanned), and redo its sampling and the numerical computations if the original solid is modified. Such methods are attractive for already existing objects acquired, for example, by various scanning devices (like laser scanner, MRI, CT, and others). Level-set methods have also an advantage of topological flexibility, useful in structural design and optimization; Wang and Wang [30] use this flexibility to design and optimize heterogeneous objects within a variational framework.

When solids are modeled with a constructive approach which is the case in some engineering fields, it would appear logical to support building the distance function in a constructive way as well.

Constructive modeling is based on applying successively set-theoretic or other operations to predefined shapes (primitives). Let two solids (point-sets in Euclidean space) be denoted by $f_1 \geq 0$ and $f_2 \geq 0$, then the union of these two objects can be defined by $f_\cup = max(f_1, f_2)$ and the intersection by $f_\cap = min(f_1, f_2)$ [1,2]. In this case, if $f_1(x, y, z)$ and $f_2(x, y, z)$ correspond to the signed distances from the point (x, y, z) to the surfaces defined by $f_1 = 0$ and $f_2 = 0$, then $f_\cup$ and $f_\cap$ correspond to approximate

distance functions for the entire complex object (see [20] for a proof that the resulting function defining the complex object is not the exact distance function but is bounded by the exact distance function). However, *min* / *max* operations result in "C^1 discontinuity" at any point where $f_1 = f_2$. It can cause unexpected results in further operations on the object such as blending, metamorphosis, and others.

There are works aiming at the replacement of *min* / *max* with smoother functions to overcome this "C^1 discontinuity": Rvachev proposed the R-functions [12], which define exact set-theoretic operations, but do not preserve the Euclidean distance value. R-functions also suffer from an exponential growth of the function value when for example the union of several overlapping solids is considered. A normalization can be applied but it approximates the distance function only close to the surface. The constructive approach of [31] relies on joining trimmed lines (for curve modeling) or trimmed triangles (for surface modeling) by R-functions. The result is then normalized to avoid bulging on the joint points. This approach can smooth the resulting distance function to any order, but at the expense of the quality of the distance approximation, which is accurate only close to the surface. This method may also involve a significant number of segments, resulting in a potentially large size for the representation. Moreover the problem of deriving a constructive representation from trimmed implicit surfaces or curves is related to the problem of boundary to CSG (Constructive Solid Geometry) conversion [32,33] and is not fully solved. The superelliptic approximations of *min* / *max* [1] do not describe exact set-theoretic operations and suit only to blending. The elliptic approximation of *min* / *max* by Barthe et al [34] is designed initially for blending and the approximation error grows infinitely far from the boundary.

1.2 Problem statement and contribution

We consider the problem of constructive modeling of heterogeneous objects, where the distance to the boundary surface of the solid and/or to the material features is used as a parameter to control the material functions. The work of [7] is extended by the proposed controlled smooth approximation of the Euclidean distance field for designing the geometry of the solid and its material attributes in a constructive way.

For this purpose, we introduce (section 2) new approximations for *min* / *max* operations inspired by the work of [34]. The new proposed functions are in C^1 on $R^2\backslash\{(0,0)\}$ and keep a bounded and controllable approximation of the *min* / *max* functions. From this point of view, we call the constructed defining function of the object by the term signed approximate real distance function (SARDF), the approximate *min* function can be called SARDF intersection, and the approximate *max* function - SARDF union.

These set-theoretic operations are used within the hypervolume constructive framework of Pasko et al. [10] and extend it for distance based modeling. In the latter model, both the geometry of the solid, and the shape of the definition domains for the attributes can be defined in constructive ways. Under the condition that primitives are defined by Euclidean distance functions (or approximation), the resulting constructive solids and attributes geometry built with the proposed operations have a smoothed distance like field as their defining function (section 3). Euclidean distance functions are available for all typical primitives of a traditional CSG system [20]. Normalized primitives (Appendix A of [31]) can also be used though the resulting distance functions will approximate the distance only close to the surface. Interpolation methods can also be used to define some complex freeform shapes as primitives.

The modified constructive hypervolume model is used to answer the question (section 5.2 of [7]) of the practical ways of computing the Euclidean distance field and then is combined with the work of [7] to model constructive heterogeneous objects with signed distance fields. Section 4 presents some examples of heterogeneous objects constructed with the proposed approach. We also provide a comparison with other existing set-theoretic operations and underline the quality and accuracy of the approximated Euclidean field (compared to R-Functions), and its smoothness (compared to *min* / *max*).

2 SARDF FRAMEWORK

Our intention is to propose a framework for modeling constructive heterogeneous objects where the Euclidean distance to the object and material features' boundary is used as a parameter to control the material distributions. The idea of parameterization of the material distribution by distance is already discussed in several works (see [7] and the various references therein), whereas the construction of the Euclidean distance function is practically not discussed.

We rely on the mathematical model introduced by Pasko et al. [10] to define heterogeneous objects. This model is reminded in the following sub-section. It is extended by primitives defined with signed Euclidean distance functions, and new formulations for the set-theoretic operations, which keep a better distance approximation than the R-functions and are smoother than *min* / *max*.

2.1 Constructive hypervolume model

The constructive hypervolume model is introduced in [10] as a mathematical model to define heterogeneous objects. A general hypervolume object is defined as a multidimensional point set G with multiple attributes given at any of its points. The attributes S_i represent abstract values or physical characteristics such as temperature, color, material distribution, etc. A representation of the hypervolume is proposed as:

$o = (G, A_1, \ldots, A_k) : (F(X), S_1(X), \ldots, S_k(X))$ where:

- $X = (x_1, \ldots, x_n)$ is a point in the n-dimensional Euclidean space E^n,

- $F : E^n \rightarrow R$ is a real-valued function of point coordinates to represent the point set *G*, based on the FRep model [11],
- $S_i : SP_i \rightarrow R$, $SP_i \subset E^n$ is a real-valued scalar function corresponding to an attribute A_i that is not necessarily continuous.

The function *F(X)* is real valued. For each given point, it is evaluated and depending on the sign of the returned value, one can classify the given point as inside, outside or on the boundary of the object. This function is represented in the modeling system by a tree structure with primitives in the leaves and operations in the nodes. The term *constructive tree* is generally used for this tree structure. The only requirement of the FRep model is that the defining function *F* is at least continuous.

Similarly, depending on the applications, the attribute functions can be defined using physical models or a constructive approach. The spatial subset, where an attribute is defined, is called a *space partition,* designated as SP_i in the above formulation. There are no definite values for an attribute outside its space partition. For each material feature, there is at least one space partition, containing this material feature. However a material feature can be contained in more than one space partition, in the case, for example, when the material feature is made of the known composition of several materials.

In the present work, the former model is extended so that each primitive is defined by the Euclidean distance function. Hart [20] provides a list of primitives with known distance functions. These primitives are used to define both the geometry of the solid and the space partitions (i.e. the spatial subset where an attribute is defined). Set-theoretic operations on primitives and complex objects are implemented with the proposed SARDF operations.

2.2 Overview of SARDF operations

Any contour line of the *min* and *max* functions has a sharp corner at the point, where the two arguments have equal value. Following the general approach of [34], we propose to replace the sharp corner in any contour line with a circular arc. Two parabolas, symmetric with respect to the line $y = x$, are used to delimit the frontier of the circular arc approximation (see Fig. 1 in the case of the smoothed *min* function).

The use of circular approximations for the *min* and *max* functions provides the smoothness property of the resulting approximate distance function for constructive shapes built using normal primitives (i.e. defined by Euclidean distance functions). We prevent the radius of the circular arc from growing infinitely by introducing a fixed threshold *R*. A bounding band is introduced by two parallel straight lines that enclose the arcs with this fixed radius. These band lines are defined by a shift of the line $y = x$ at *R* distance in positive and negative *x* directions: $y = x - R$ and $y = x + R$ (see Fig. 1). This bounding band provides a fixed upper limit of the error compared to the *min* / *max* approach at any given point.

The two branches of the parabolas are defined to be tangent to the two parallel lines $y = x - R$ and $y = x + R$ at the connecting points *(R, 2R)* and *(2R, R)* and pass through the origin *(0,0)*; it gives the expressions for these two parabolas: $y = \frac{x^2}{4R}$ and $x = \frac{y^2}{4R}$. Note that the use of parabolas to restrict the circular approximation ensures that the constructed function is C^1 on the arc of circle A_1A_2.

The resulting defining functions of shapes are built using normal primitives and the newly introduced set-theoretic operations called SARDF operations. The union operation is called SARDF union (we use the symbol "$\cup_S$") and the intersection operations is called SARDF intersection (with the symbol "$\cap_S$").

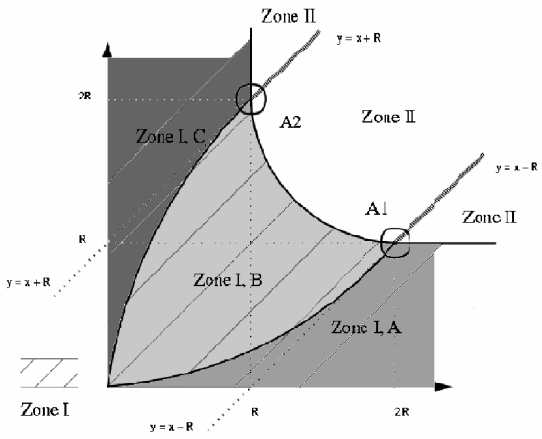

Figure 1: The first quadrant is divided into two zones. The growing circular approximation is applied in zone I, whereas we introduce a fixed radius approximation with the bounding band in zone II.

2.3 SARDF intersection of arbitrary objects

2.3.1 Construction of the intersection function

The main steps of the construction of the smoothed intersection in the first quadrant ($x > 0$ and $y > 0$) are given. By symmetry, the construction in the third quadrant ($x < 0$ and $y < 0$) is similar. In the two other quadrants, the expression for the intersection is equal to the *min* function.

Zone I, B Given a point *(x, y)* in the first quadrant we consider the first case when it is in zone I, B in Fig. 1 and calculate the iso-level value *d* for the smoothed intersection function at this point. The given point belongs to a circular arc that is tangentially connected to two horizontal and vertical rays when reaching the parabola (see Fig. 1). The equation of this arc is $(x - x_0)^2 + (y - y_0)^2 = r^2$, where x_0, y_0 and *r* need to be expressed as functions of the searched value *d*. The point at the intersection of the parabola and the iso-level *d* of the

searched function, is at a distance d from the axis $y = 0$. This point belongs also to the parabola, so it satisfies $d = \frac{x_0^2}{4R}$, and by symmetry: $d = \frac{y_0^2}{4R}$.
The coordinates of the center of the circular arc (x_0, y_0) satisfy: $x_0 = y_0 = d + r$; it follows that $r = y_0 - d = 2\sqrt{Rd} - d$. Using the substitution of variables $\sqrt{d} = z$ and expanding the equation of the circular arc, we obtain the following algebraic equation:

$$z^4 - 4\sqrt{R}z^3 - 4Rz^2 + 4\sqrt{R}(x+y)z - (x^2+y^2) = 0 \quad (1)$$

Thus in the first quadrant, in the zone I, B, the expression of the intersection is the square of one of the four roots of the algebraic equation (1). The roots of an algebraic equation of degree four are known algebraically. The root of interest is found by using one of the limit conditions, for example $d(2R,R) = R$.

Zone II, inside the bounding band Given a point (x, y) in zone II, within the bounding band (see Fig. 1), the iso-level value d of the smoothed intersection function at that point is searched. This point belongs to a circular arc that is tangentially connected to two horizontal and vertical rays when reaching the two lines of the bounding band. The equation of this circular arc is: $(x - x_0)^2 + (y - y_0)^2 = R^2$. Note that R is a constant, only x_0 and y_0 need to be expressed as functions of d.
The coordinates (x_0, y_0) of the circular arc satisfy: $x_0 = y_0 = d + R$. After substitution into the equation of the circular arc and expanding this equation, d is obtained as one of the two solutions of the following algebraic equation:

$$2d^2 + d(4R - 2x - 2y) + (x^2 + y^2 - 2R(x+y) + R^2) = 0 \quad (2)$$

The root of interest is obtained by using the limit condition: $d(2R, R) = R$.

Zone I, A and C and II outside the bounding band The expression of the intersection is exactly equal to *min* in these areas.

2.3.2 Expression for the intersection operation

Let $f_1(x,y,z)$ and $f_2(x,y,z)$ be the distance functions defining two objects. The intersection between these two objects is defined following the previous method with the substitution $x \rightarrow f_1(x,y,z)$ and $y \rightarrow f_2(x,y,z)$. The general expression for the SARDF intersection function of f_1 and f_2 can be described as follows:

Case 1: $f_1 > 0$ **and** $f_2 > 0$ In the current paragraph, E_1 is used for the following boolean expression: $E_1 = (f_1 < R$ or $f_2 < R$ or $(f_1 < 2R$ and $f_2 < 2R$ and $(f_1 - 2R)^2 + (f_2 - 2R)^2 > R^2))$.

- If E_1 and $f_2 > \frac{f_1^2}{4R}$ and $f_1 > \frac{f_2^2}{4R}$, $f_1 \cap_S f_2 = z^2$, where z is the root of (1) verifying $z^2(2R,R)=R$;
- if E_1 and $f_2 \le \frac{f_1^2}{4R}$, $f_1 \cap_S f_2 = f_2$
- if E_1 and $f_1 \le \frac{f_2^2}{4R}$, $f_1 \cap_S f_2 = f_1$
- if $\neg E_1$ and $f_1\text{-}R < f_2 < f_1 + R$, $f_1 \cap_S f_2 = \frac{1}{2a}(-b + \sqrt{b^2 - 4ac})$, where $a = 2$, $b = -2f_1 - 2f_2 + 4R$, and $c = f_1^2 + f_2^2 - 2f_1R - 2f_2R + R^2$;
- if $\neg E_1$ and $f_2 \le f_1\text{-}R$, $f_1 \cap_S f_2 = f_2$
- if $\neg E_1$ and $f_2 \ge f_1+R$, $f_1 \cap_S f_2 = f_1$

Case 2: $f_1 \le 0$ **and** $f_2 \ge 0$
$f_1 \cap_S f_2 = f_1$

Case 3: $f_1 < 0$ **and** $f_2 < 0$ We denote by E_2 the following boolean expression: $E_2 = (f_1 > -R$ or $f_2 > -R$ or $(f_1 > -2R$ and $f_2 > -2R$ and $(f_1 + R)^2 + (f_2 + R)^2 < R^2))$.

- if E_2 and $f_2 < -\frac{f_1^2}{4R}$ and $f_1 < -\frac{f_2^2}{4R}$, $f_1 \cap_S f_2 = z$, where z is the root of $\frac{d^4}{16R^2} - \frac{d^3}{2R} + \frac{1}{2R}d^2(f_1 + f_2 - 2R) + (f_1^2 + f_2^2) = 0$ verifying z(-2R,-R)=-2R;
- if E_2 and $f_2 \ge -\frac{f_1^2}{4R}$, $f_1 \cap_S f_2 = f_2$
- if E_2 and $f_1 \ge -\frac{f_2^2}{4R}$, $f_1 \cap_S f_2 = f_1$
- if $\neg E_2$ and $f_1\text{-}R < f_2 < f_1 + R$, $f_1 \cap_S f_2 = \frac{1}{2a}(-b + \sqrt{b^2 - 4ac})$, where $a = 2$, $b = -2f_1 - 2f_2 + 4R$, and $c = f_1^2 + f_2^2 - 2f_1R - 2f_2R + R^2$;
- if $\neg E_2$ and $f_2 \le f_1\text{-}R$, $f_1 \cap_S f_2 = f_2$
- if $\neg E_2$ and $f_2 \ge f_1+R$, $f_1 \cap_S f_2 = f_1$

Case 4: $f_1 \ge 0$ **and** $f_2 \le 0$

$f_1 \cap_S f_2 = f_2$

2.4 Smoothness of the SARDF intersection

We give the main points of the proof that the function SARDF intersection is in C^1 on $R^2 \setminus \{(0,0)\}$. At $(0,0)$ the function is continuous only.
In the quadrants II and IV the function is C^1. The proof is similar in the quadrants I and III, so it is given only in the first quadrant.
First, we note that in each zone of the first quadrant, the different parts of the function are C^1. The problems of continuity of the function and the partial derivatives may appear at the boundaries between the different

expressions, i.e., on the branches of the parabolas, the straight lines ($y = x - R$ and $y = x + R$), and on the circular arc boundary A_1A_2 between the growing radius zone and the fixed radius zone. The function is symmetric with respect to the line $y = x$, thus only the part of the first quadrant below $y = x$ needs to be considered.
Note that for two general objects defined by $f_1(x,y,z)$ and $f_2(x,y,z)$, the partial derivatives are obtained with the substitution $x \rightarrow f_1(x,y,z)$ and $y \rightarrow f_2(x,y,z)$, and the Jacobian of $(f_1(x,y,z), f_2(x,y,z))$. The smoothness of the constructed object is dependent on the smoothness of f_1 and f_2.

2.4.1 SARDF intersection is continuous

At the parabolic boundary, Let $P = (x, y) = (u, \frac{u^2}{4R})$, with $u \in [0, 2R]$ be a point on the parabola arc, the value of the function in zone I, A, at that point is $y = \frac{u^2}{4R}$. We need to check that this value at P matches with the value of the function in Zone I, B at that point, given by equation (1). It is easy to check that for $(x, y) = (u, \frac{u^2}{4R})$, and with $z = \sqrt{d} = \frac{u}{2\sqrt{R}}$, the algebraic relation (1) holds. We can conclude with the continuity of the SARDF expression at the parabolic boundary.

At the line $y = x - R$, Let $P = (x, y) = (u, u-R)$, with $u \in [2R, \infty[$, be a point on the straight line, the value of the function in zone II, outside the bounding band at P is $y = u - R$. Again we check that this value at P matches with the value of the expression within the boundary band, zone II, given by equation (2). It is easy to check that for $P = (x, y) = (u, u-R)$, $d = u - R$ satisfies equation (2), we can conclude with the continuity of the SARDF expression at this boundary.

At the circular arc boundary A_1A_2, let $P=(x, y)=(2R+R\cos(u),2R+R\sin(u))$, with $u \in \left[\frac{5\pi}{4}, \frac{3\pi}{2}\right]$, be a point on that circular arc. The value of the function at P is given by its value at the point A_1 and is $y = R$. We check that this value matches the value of the expressions in the zones I, B and II at P, by checking that equations (1) and (2) hold. Again, after applying some calculus, the relations (1) and (2) hold and we can conclude with the continuity at that boundary.

2.4.2 SARDF intersection is C^1

To prove it, we verify that the value of the partial derivatives match on the boundary points. First, the equation (1) and (2) are used to obtain expressions for the partial derivatives of the function in the zones I, B and II, within the boundary.

Expression for the partial derivatives in zone I, B: In zone I, B, the square root of the function SARDF intersection $\sqrt{d}$ satisfies the algebraic equation (1). Taking the partial derivative with x of (1) gives:

$$4\frac{\partial z}{\partial x}z^3 - 12\sqrt{R}\frac{\partial z}{\partial x}z^2 - 8R\frac{\partial z}{\partial x}z + 4\sqrt{R}(x+y)\frac{\partial z}{\partial x} + 4\sqrt{R}z - 2x = 0$$

It follows that: $\frac{\partial z}{\partial x} = \frac{2x - 4\sqrt{R}z}{4z^3 - 12\sqrt{R}z^2 - 8Rz + 4\sqrt{R}(x+y)}$.
Since $z = \sqrt{d}$, it comes that $\frac{\partial z}{\partial x} = \frac{1}{2}\frac{\partial d}{\partial x}\frac{1}{\sqrt{d}}$. Combining it with the previous expression, we get the following relation for the partial derivative of the function in zone I, B

$$\frac{\partial d}{\partial x} = 2\sqrt{d}\,\frac{2x - 4\sqrt{R}z}{4z^3 - 12\sqrt{R}z^2 - 8Rz + 4\sqrt{R}(x+y)} \quad (3)$$

with $z(x,y) = \sqrt{d(x,y)}$.
By the same procedure, we obtain an expression for the partial derivative by y in zone I,B:

$$\frac{\partial d}{\partial y} = 2\sqrt{d}\,\frac{2y - 4\sqrt{R}z}{4z^3 - 12\sqrt{R}z^2 - 8Rz + 4\sqrt{R}(x+y)} \quad (4)$$

with $z(x,y) = \sqrt{d(x,y)}$.

Expression for the partial derivatives in zone II, within the bounding band: In zone II, within the bounding band, the function satisfies equation (2). With the same method as above, we take the partial derivative by x gives: $4\frac{\partial d}{\partial x}d + \frac{\partial d}{\partial x}(4R - 2x - 2y) - 2d + (2x - 2R) = 0$.
It follows that:

$$\frac{\partial d}{\partial x} = \frac{2d - 2(x - R)}{4d + (4R - 2x - 2y)} \quad (5)$$

Similarly an expression for the partial derivative by y can be obtained:

$$\frac{\partial d}{\partial y} = \frac{2d - 2(y - R)}{4d + (4R - 2x - 2y)} \quad (6)$$

Expression for the partial derivatives in zone I, A and zone II, below $y = x-R$**:** The function is exactly *min* in these two areas, and so the partial derivative in the x direction is 0 and 1 in the y direction.

"C^1 continuity" at the parabolic arc: Let $P = (x, y)$

$=(u, \frac{u^2}{4R})$, with $u \in [0, 2R]$, be a point on the arc, at P, $z = \sqrt{d} = \frac{u}{2\sqrt{R}}$; it is easy to verify that at P equations (3) and (4) give: $\frac{\partial d}{\partial x} = 0$ and $\frac{\partial d}{\partial y} = 1$.

"C^1 continuity" at the line $y = x - R$: Let $P = (x, y) = (u, u-R)$, with $u \in [2R, \infty[$ be a point on the line, at P, $d = u - R$; it is easy to verify that at P equations (5) and (6) give: $\frac{\partial d}{\partial x} = 0$ and $\frac{\partial d}{\partial y} = 1$.

"C^1 continuity" at the circular arc boundary: Let $P=(x, y)=(2R+R\cos(u), 2R+R\sin(u))$, $u \in \left[\frac{5\pi}{4}, \frac{3\pi}{2}\right]$ be a point on the circle boundary between the growing radius zone and the constant radius zone. At P, the value of the function is R. Using these informations in equation (3), we obtain after straightforward calculus $\frac{\partial d}{\partial x} = \frac{\cos(u)}{\cos(u) + \sin(u)}$. Similarly, with equation (5): $\frac{\partial d}{\partial x} = \frac{\cos(u)}{\cos(u) + \sin(u)}$.

Similarly for the partial derivative $\frac{\partial d}{\partial y}$, equation (4) gives: $\frac{\partial d}{\partial y} = \frac{\sin(u)}{\cos(u) + \sin(u)}$, and equation (6) gives: $\frac{\partial d}{\partial y} = \frac{\sin(u)}{\cos(u) + \sin(u)}$.

With the equality of the partial derivatives we can conclude that the SARDF intersection is C^1 on the boundary circular arc. It is still C^1 at A_1, with $u = \frac{3\pi}{2}$.

3 COMPARISON OF SARDF WITH OTHER SET-THEORETIC OPERATIONS

3.1 Time comparison

We look at the time efficiency of SARDF union and intersection and the overhead in time compared to *min* / *max* and the R-functions union and intersection.

According to the tests, we found a factor of approximately 6 between SARDF union and *max*, 5.5 between SARDF intersection and *min*, 3.5 between SARDF union and R-function union and 2.9 between SARDF intersection and R-function intersection. The sampling of the SARDF intersection on a 20001*20001 grid takes 29.5 seconds (5.537 for max, and 10.074 for the R-function). This sampling corresponds to sampling a model with 400 intersection operations on a 100*100*100 grid. All the functions in the tests were implemented in C language on a Pentium 4 processor 1.7 GHz, with 256 MBytes of RAM. No particular optimization was used in the code, learning room for improvement.

3.2 Qualitative comparison of the union operations: SARDF union, max, and R-union

We qualitatively compare the three union operations *max*, R-union, and SARDF union applied in constructive modeling in terms of the quality of approximation of the Euclidean distance for the resulting function, and in terms of the smoothness of this function. The solid used in the experiments is the union of two ellipsoids centered at (5, 0, 0) and (5, 0, -5) with respective radii (5, 2, 2) and (2, 2, 5).

Let f_1 and f_2 be the signed Euclidean distance functions defining the two ellipsoids. The interior of an ellipsoid corresponds to $f_i > 0$ and the exterior to $f_i < 0$. The surface boundary of an ellipsoid corresponds to $\{X \in R^3: f_i(X)=0\}$. The procedure used for computing the exact signed distance from a point in R^3 to the surface of an ellipsoid is discussed in [35].

We are interested in the quality of the approximation of the Euclidean distance function and the smoothness of $f_1 \cup f_2$, where $\cup$ stands for the functional definition of one of the three union operations. The expression used for the R-union of two objects is $f_1 \cup f_2 = f_1 + f_2 + \sqrt{f_1^2 + f_2^2}$.

Figure 2 shows the contour maps of a cross-section by the plane $y = 0$ of the resulting defining functions for different analytical expressions for union.

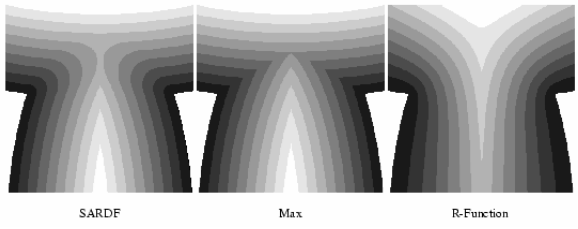

Figure 2. Contour maps of the union of two ellipsoids for the three different union operations. The level of gray corresponds to range of approximate distances from points inside the solid to its surface. Left: SARDF union, middle: *max*: sharp corners indicate points of derivatives discontinuity, right: R-union: contour map of the function clearly shows that the resulting function loses the distance like behaviour quite close to the boundary even with exact distance functions used for the arguments.

Figures 2 left, middle and right show some interior contour lines of the function for the considered object. The figures correspond to the models made respectively with SARDF union, *max*, and R-function union. The contour map of the defining function built with R-union loses the Euclidean distance like behavior quite close to the surface boundary even with exact distance functions defining the two ellipsoids. This loss of the distance like

property is emphasized with the comparison to the maps given by using SARDF union and *max* (Fig. 2 left and middle). These contour maps have very similar contour lines except at the points joining the contour lines of the two functions, which are sharp for *max* (see Fig. 2 middle) and smooth for SARDF (see Fig. 2 left). It illustrates the discontinuity of the partial derivatives of the function defining the solid and built using *max*.
Points of discontinuity of the Euclidean distance's partial derivatives are also present on the main axis of each ellipsoid (Fig. 2). It is known that as soon as at least two points of the shape have equal distance values to the given point in space, the Euclidean distance function has a discontinuity of its partial derivatives at this point. This set of points is known as the medial axis of a shape. The discontinuity of the partial derivatives at these points remains independantly of the analytical expression used for the union operation.
So far, we have illustrated two properties: the SARDF operations do not introduce additional points where the resulting function is not C^1, like *min* / *max*; and they are better approximations of the Euclidean distance than the R-functions. Both these properties are important in heterogeneous object modeling: Shin and Dutta relate that R-function is not an exact distance function, consequently making it difficult for a designer to predict or control the material distribution (section 3.3 p. 210 and Figure 10, p. 211 of [36]). Biswas et al report that the lack of smoothness in a material function parameterized by the distance result in zones of concentration or stress of the materials (section 1.3 of [7]).

4 CONSTRUCTIVE HETEROGENEOUS OBJECTS MODELING WITH SARDF

We propose some examples to illustrate the use of the SARDF operations and normal primitives in constructive heterogeneous modeling. The SARDF operations are used instead of the R-functions or the *min* / *max* functions in the different constructive trees to define the geometry of the solid and the space partitions where attributes are defined.
A normal primitive, is a primitive with a defining function *f*, which at a given point $X \in R^3$, returns the Euclidean distance from X to the surface $f^{-1}(0)$. Primitives with known expressions for the distance are given in [20].
We show how the different expressions for the set-theoretic operations affect the material distributions and their properties.

4.1 Two-dimensional example

At first, we illustrate the use of SARDF in modeling a two-dimensional heterogeneous object. The geometry of the object (Fig. 3) is defined as $f(X) \geq 0$, where *f* is evaluated by traversing the constructive FRep tree [11] with a box and a cylinder in the leaves, and the subtraction operation in the node.

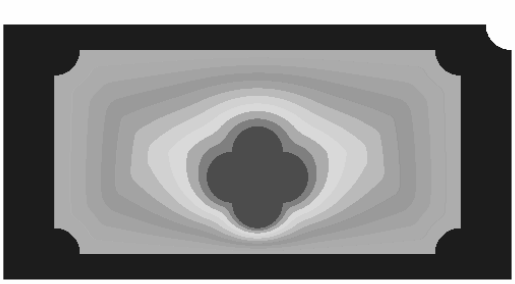

Figure 3. A two-dimensional CAD part with three different material regions (blue: material 1, red: material 2, color gradient: functionally graded material.

This object is made of two materials and three material regions (Fig. 3). We use the notation $m_1(X)$ and $m_2(X)$ for the scalar volume fraction component of the materials 1 and 2. For visualization purposes, the material distributions are mapped to the "RGB" color space: a color is attributed to each material and the final color is the combination of the colors corresponding to each material, weighted by the scalar volume fraction.
Two of the three material regions correspond to regions where there is only material 1 uniformly distributed (blue in Fig. 3) and there is only material 2 uniformly distributed (red in Fig. 3) correspondingly. The last material region corresponds to functionally graded material. The geometry of each region is defined using FRep in a constructive way, similarly to the shape's geometry. SARDF operations are used in the nodes and normal primitives in the leaves of the constructive tree. The resulting functions provide C^1 approximation of the distance to each material region. These distances are used to specify the functionally graded material.
The scalar volume fraction of each component material in the functionally graded material region is given by: $m_1(X)=w_1(X)M_1$ and $m_2(X)=w_2(X)M_2$, where M_1 and M_2 stand for the value of the scalar volume fraction on the boundary of the first and second material features shown respectively in blue and red Fig. 3.
The weighting functions $w_1(X)$ and $w_2(X)$ are defined using a normalization of each inverse distance functions:

$$w_1(X) = \frac{\frac{1}{d_1(X)}}{\frac{1}{d_1(X)} + \frac{1}{d_2(X)}} = \frac{d_2(X)}{d_1(X) + d_2(X)} \quad (7)$$

$$w_2(X) = \frac{\frac{1}{d_2(X)}}{\frac{1}{d_1(X)} + \frac{1}{d_2(X)}} = \frac{d_1(X)}{d_1(X) + d_2(X)} \quad (8)$$

where $d_1(X)$ and $d_2(X)$ are the distances from point X to the boundary of respectively the material features shown in blue and red Fig. 3.
These two distance maps are illustrated in Fig. 4 and Fig. 5. Fig. 4, left and Fig. 4, right correspond respectively to the approximate distance map d_1 when the R-functions and the SARDF operations are used correspondingly to define the shape. In a similar way, Fig. 5, left and Fig. 5, right correspond to the approximate distance d_2 when using R-functions and SARDF.
The approximate distance maps built using R-functions

indicate that even if R-functions have good smoothness properties, they do not provide a good approximation to the distance function, making it difficult to precisely control the material distribution.

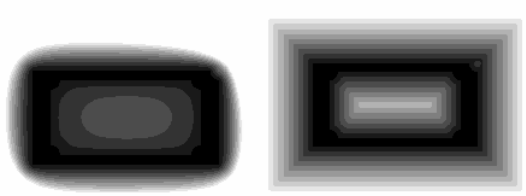

Figure 4. Approximate distance map d_1 from point X to the boundary of the region where only material 1 exists. Left: using R-functions. Right: using SARDF operations.

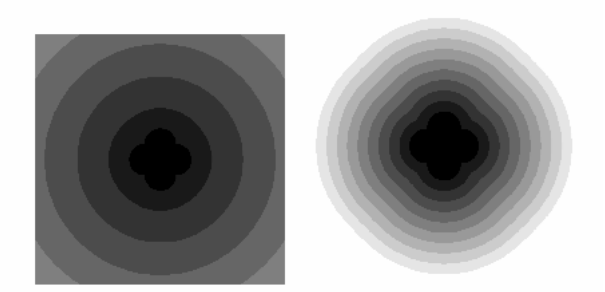

Figure 5. Approximate distance map d_2 from point X to the boundary of the region where only material 2 exists. Left: using R-functions. Right: using SARDF operations.

The weighting functions $w_1(X)$ and $w_2(X)$ are continuous and satisfy the interpolation condition $w_i(\partial B_j) = \delta_{ij}$, with $1 \le i,j \le 2$, δ_{ij} is the Kronecker symbol, and ∂B_j are the boundaries of the material features seen in blue and red Fig. 4. The functions $w_1(X)$ and $w_2(X)$ form a partition of unity.

The properties of these functions are illustrated in Fig. 6 with a cross section of the model through the y-axis and the visualization of the evolution of the weighting functions $w_1(X'=(X,const))$ and $w_2(X')$ along the x-axis. Note that in the current example m_1 and m_2 have the same graphs, since the values of the volume fraction on the boundaries, M_1 and M_2 have been chosen equal to 1.

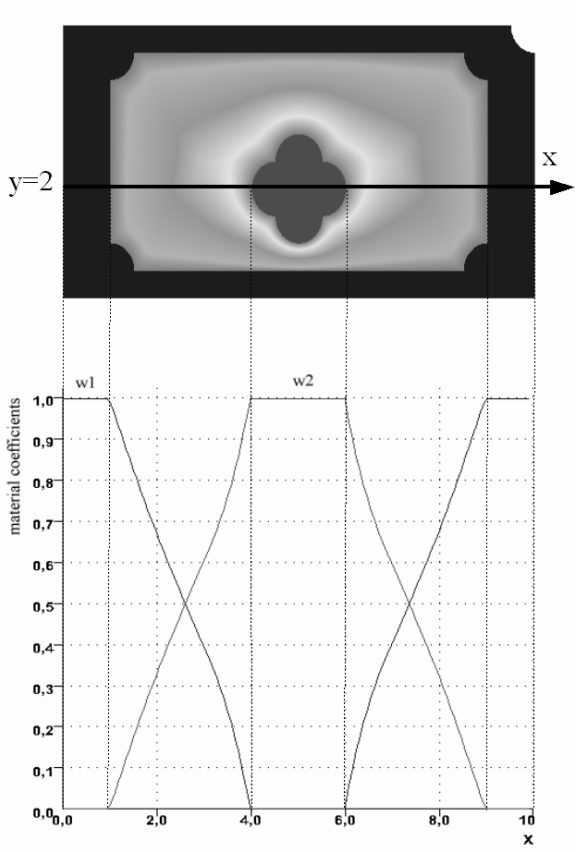

Figure 6. A cross section parallel to x-axis and the distribution of the materials in the cross section for the CAD part constructed with SARDF functions.

One can notice (Fig. 6) a "C^1 discontinuity" at the points on the boundary of the material features. This can cause the same problems as the distance function "C^1 discontinuity". Fortunately, these sharp corners can be smoothened by a modification of the expressions for the coefficients (Eq. (7) and (8)). The expressions used for the material feature weights correspond to a particular case of the inverse distance weighting [37]. More general expressions are:

$$w_1(X) = \frac{d_2^k(X)}{d_1^k(X) + d_2^k(X)} \quad \text{and} \quad w_2(X) = \frac{d_1^k(X)}{d_1^k(X) + d_2^k(X)} \quad .$$

The case $k=1$ gives Eq. (7) and (8). The parameter k controls the smoothness of the functions on the points of the material features.

Replacing every SARDF operation by an R-function or *min* / *max* in the constructive trees for the geometry of the solid and the material regions gives different material distributions in the same cross-section (see Fig. 7, left and 7 right).

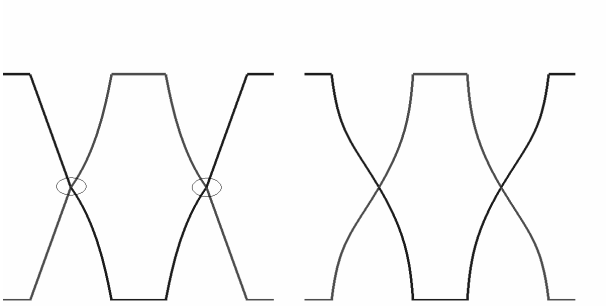

Figure 7. Material distributions in the cross-section $y = 2$ for materials 1 and 2 using: R-functions in the constructive trees for the geometry of the solid and the material regions (right). *min* / *max* in the constructive trees for the geometry of the solid and the material regions (left). The circled points correspond to points of C^1 discontinuity of the material distributions.

Figures 7, left and right reflect at the level of the material distribution the problems of using the R-functions, or *min* / *max* in constructive heterogeneous modeling. Figure 7, right shows the role played by the accuracy of the distance approximation when the distance is used to parameterize the material distributions. The unpredictable behaviour of the distance approximation makes the task of the designer difficult. For example, we would expect that the first part of the blue curve (just before the intersection with the red curve) is linear. This "bad behaviour" of the R-functions was noticed by Shin and Dutta in [36].

Figure 7, left illustrates the "C^1 discontinuity" of the *min* (and *max*) functions and its impact on the material distribution. Both distributions of material 1 (blue) and 2 (red) have two points of "C^1 discontinuity" (circled in Fig. 7, left). It results in problems of stress or concentrations as noticed by Biswas et al in [7].

Using SARDF for the set-theoretic operations does not introduce new points of C^1 discontinuity, and keeps a good approximation of the distance; these properties can be seen consequently in the graph of the material distributions (Fig. 6).

In this and in the following examples only two materials are in the overlapping zone. More materials can be blended and the expressions for inverse distance weighting (Eq. (7) and (8)) can be extended to the case where more than 2 materials are blended. Additional details on the inverse distance weighting used for the interpolation of materials defined over functionally defined sets can be found in [38]. More complex expressions for compositions of multiple materials, like vector valued materials, constrained and weighted interpolation of materials can be found in [7].

The resulting model of the CAD part and its material distribution is illustrated by Fig. 3. The distribution of the material 1, given by its scalar volume fraction $m_1(X)$ is mapped to the blue color, and the distribution of the material 2, given by $m_2(X)$ to the red color. Stripes are used to make the visualization of the changes in material distribution easier.

4.2 Three-dimensional CAD part

We propose a second example (in three-dimensional space) with more complex shapes for the geometry of the object and the geometry of the regions corresponding to the material features. With this example, we underline the fact that complex shapes can be made using SARDF operations and normal primitives.

The overall geometry of the object is a block with two (constant) material features inside. We keep the same notation as in the previous subsection, with $m_1(X)$ and $m_2(X)$ the scalar volume fraction of the materials 1 and 2. Figure 8, top, left shows the first material feature corresponding to the material 1 (in blue); it is cut by a planar half-space for visualization purposes only. Figure 8, top, middle shows the second material feature (in red); its geometry is composed of blocks and ellipsoids, combined with SARDF unions and intersections. Fig. 8, top, right, illustrates a zoom to one of the pins. Such a pin is modeled with ellipsoids as primitives and SARDF union and intersection as operations: it is the SARDF union of four ellipsoids, which are after subtracted from a fifth ellipsoid.

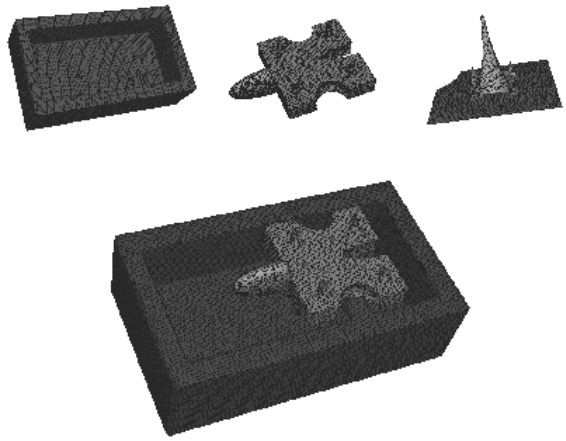

Figure 8. Top, left: the first material feature, top, middle: the second material feature, with a zoom on one of the pins, on the right (top, right), bottom: union of the two material features.

To express the material behaviour in the region between the two material features (this region can be seen in Fig. 10, bottom), we use the equations (7) and (8) for the weights for each material feature. It indicates that the closest material feature has the strongest influence. The overall distribution of the materials is shown in Fig. 9, left. The geometry corresponding to the second material feature is rendered, using a red color, then for the visualization of the material distribution, two cross-sections are made: one for $x=0$ and one for $z=0$. For each of the cross-section, the evolution of the material distribution is projected. For visualization purposes, each material is mapped to one color. The first material corresponds to the blue color and the second material to the red.

Figure 9, right shows a zoom to one of the pins. The geometry of the second material feature is drawn in 3D with red color. Two more cross sections with distribution of materials are added. The gradient of color expresses

the evolution of the distribution of the material composition, indicating percentage of the first and second material.

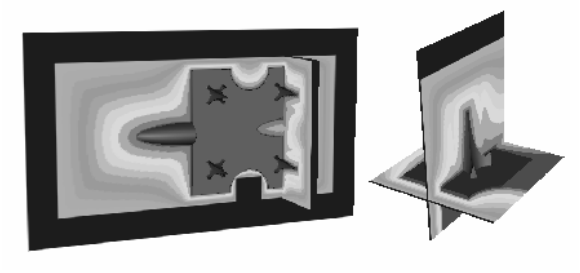

Figure 9. Distribution of two materials. Blue color corresponds to material 1, red color to material 2. The color variation indicates the fraction of each material. Left: Two cross sections are made for $x=0$ and $y=0$ to show the material distribution. Right: A zoom is made to one of the pins with two additional cross-sections.

5 CONCLUSION

5.1 Advantages of the SARDF framework in constructive heterogeneous object modeling

The core of this work is the introduction and application of special functions describing set-theoretic operations for constructive modeling. Under the condition that the primitives in use are defined by exact distance functions, the proposed set of functions provides a good approximation of the real distance value. These functions serve for defining both the geometry of the object and the geometry of regions where the materials are distributed.

The result of any constructive modeling, involving signed approximate real distance functions (SARDF) and primitives defined by distance functions, is at least C^1, except for the cases when both of the arguments of the SARDF operation are equal to 0 (surface-surface intersection curves), or for the points belonging to the medial axis of one of the primitives.

Compared to the known R-functions, the proposed SARDF operations provide better approximations for the Euclidean distance. In contrary to *min* / *max*, they do not introduce extra points of "C^1 discontinuity". Therefore they seem extremely useful in constructive modeling of heterogeneous objects, where both the geometry of the object and the material features are defined constructively using normal primitives and SARDF operations.

Our approach is a possible solution to the open question from [7] on computing the distance fields used to parameterize the distance distributions. We extend the constructive hypervolumes framework [10] to constructive design of shapes by signed distance functions, with direct applications in constructive heterogeneous modeling using the complete description of material design from [7].

Through the case studies, the viability of the proposed functions for constructive heterogeneous modeling is confirmed. The provided examples can be easily extended with more complex material distribution for the material features and more complex scheme for combination of the different attributes, since no restrictions prevent it in our model.

5.2 Extensions and research directions

In retrospect, one of the reasons for not using *min* / *max* in constructive modeling is the introduction of points of C^1 discontinuity. But as noticed earlier, such points may appear in the normal primitives due to the definition of the distance function. Some special treatment of the normal primitives is a source for future work.

We stated in the introduction that using *min* / *max* is keeping only an approximation of the exact distance field for the resulting function. Whether *min* or *max* is used, an approximation for the resulting distance field occurs in only one of the four quadrants, where the sharp edge of every contour line should be replaced by a circular arc with the opening of the arc given by the angle between the normals of both parameter shapes. The error between *min* / *max* or between the SARDF function and the exact distance field should be more carefully studied from the mathematical point of view.

The distance property of shapes and material features obtained by the proposed framework could be used to generate better quality mesh for finite element analysis using the algorithms for surface and volume discretization of FRep heterogeneous objects described in [39].

6 ACKNOWLEDGMENTS

The authors acknowledge the reviewers for fruitful comments. P.-A. Fayolle acknowledges support by Monbukagakusho, the Japanese ministry of Education, Culture, Sports, Science and Technology.

7 REFERENCES

[1] Ricci, A., 1973, "A Constructive Geometry for Computer Graphics", The Computer Journal, 16(2), pp.157–160.

[2] Sabin, M., 1968, "The Use of Potential Surfaces for Numerical Geometry", Technical Report VTO/MS/153.

[3] Kumar, V., and Dutta, D., 1997, "An Approach to Modeling Multi-Material Objects", Fourth Symposium on Solid Modeling and Applications, pp. 336-345.

[4] Kumar, V., Burns D., Dutta D., and Hoffman C., 1999, "A Framework for Object Modeling", Computer-Aided Design, 31(9), pp. 541-546.

[5] Bhashyam, S., Shin, K. H., and Dutta, D., 2000, "An Integrated Cad System for Design of Heterogeneous Objects", Rapid Prototyping Journal, 6(2), pp. 119-135.

[6] Chen, K., and Feng, X., 2003, "Computer-Aided Design Method for the Components Made of Heterogeneous Materials", Computer-Aided Design, 35(5), pp. 453-466.

[7] Biswas, A., Shapiro, V., and Tsukanov, I., 2004, "Heterogeneous Material Modeling with Distance

Fields", Computer Aided Geometric Design, 21(3), pp. 215-242.
[8] Requicha, A., 1980, "Representations for Rigid Solids: Theory, Methods, and Systems", ACM Computing Surveys, 12(4), pp.437-464.
[9] Nielson, G., 2000, "Volume Modelling", Volume Graphics, M. Chen, A. Kaufman, R. Yagel, Eds., Springer-Verlag, pp. 29-48.
[10] Pasko, A., Adzhiev, V., Schmitt, B., and Schlick, C., 2001, "Constructive Hypervolume Modeling", Graphical Models, 63(6), pp. 413-442.
[11] Pasko, A., Adzhiev, V., Sourin, A., and Savchenko, V., 1995, "Function Representation in Geometric Modeling: Concept, Implementation and Applications", The Visual Computer, 11(8), pp. 429-446.
[12] Rvachev, V., 1963, "On the Analytical Description of some Geometric Objects", Ukranian Academy of Sciences, 153(4), pp. 765-767.
[13] Qian, X., and Dutta, D., 2001, "Physics Based B-Spline Heterogeneous Object Modeling", In *ASME Design Engineering Technical Conference,* Pittsburgh.
[14] Jackson, T. R., 2000, "Analysis of Functionally Graded Material Object Representation Methods", PhD thesis, MIT, Ocean Engineering Department.
[15] Siu, Y. K., and Tan, S. T., 2002, "Modeling the Material Grading and Structures of Heterogeneous Objects for Layered Manufacturing", Computer-Aided Design, 34, pp. 705-716.
[16] Liu, H., Cho, W., Jackson, T. R., Patrikalakis, N. M., and Sachs, E. M., 2000, "Algorithms for Design and Interrogation of Functionally Gradient Material Objects", In *Proceedings of ASME 2000 IDETC/CIE 2000 ASME Design Automation Conference,* Baltimore, MD.
[17] Frisken, S., Perry, R., Rockwood, A., and Jones, T., 2000, "Adaptively Sampled Distance Fields: a General Representation of Shape for Computer Graphics", In *Proceedings of the 27th annual conference on Computer graphics and interactive techniques*, ACM Press/Addison-Wesley Publishing Co., pp. 249-254.
[18] Cohen-Or, D., Levin, D., and Solomovic, A., 1998, "Three-Dimensional Distance Field Metamorphosis", ACM Transaction on Graphics, 17(2), pp. 116-141.
[19] Jones, M. and Chen, M., 1994, "A New Approach to the Construction of Surfaces from Contour Data", Computer Graphics Forum, 13(3), pp. 75-84.
[20] Hart, J., 1996, "Sphere Tracing: A Geometric Method for the Antialiased Ray Tracing of Implicit Surfaces", The Visual Computer, 12(10), pp. 527-545.
[21] Zhou, Y., Kaufman, A., and Toga, A., 1998, "3d Skeleton and Centerline Generation Based on an Approximate Minimum Distance Field", The Visual Computer, 14(7), pp. 303-314.
[22] Goldman, R. N., 1983, "Two Approaches to a Computer Model for Quadric Surfaces", IEEE Computer Graphics and Applications, 3(6), pp. 21-24.
[23] Satherley, R., and Jones, M., 2001, "Hybrid Distance Field Computation", Volume Graphics, pp. 195-209.
[24] Zhao, H., 2005, "A Fast Sweeping Method for Eikonal Equations", Mathematics of Computation, 74, pp. 603-627.
[25] Tsai, Y. R., 2002, "Rapid and Accurate Computation of the Distance Function Using Grids", Journal of Computational Physics, 178(1), pp. 175-195.
[26] Roessl, C., Zeilfelder, F., Nurnberger, G., and Seidel, H.-P., 2004, "Spline Approximation of General Volumetric Data", ACM Solid Modeling 2004.
[27] Sethian, J., 1999, *Level-Set Methods and Fast Marching Methods*. Cambridge University Press.
[28] Zhao, H., Osher, S., and Fedkiw, R., 2001, "Implicit Surface Reconstruction and Deformation Using the Level-Set Method", In *the 1st IEEE workshop on variational and level-set methods in computer vision, Canada.*
[29] Ohtake, Y., Belyaev, A., Alexa, M., Turk, G., and Seidel, H.-P., 2003, "Multi-Level Partition of Unity Implicits", ACM Transaction on Graphics, 22(3), pp. 463-470.
[30] Wang, M. Y., Wang, X., 2005, "A Level-Set Based Variational Method for Design and Optimization of Heterogeneous Objects", Computer Aided Design, special issue on "Heterogeneous Object Models and their Applications", 37(3), pp. 321-337.
[31] Biswas, A., and Shapiro, V., 2004, "Approximate Distance Fields with Non-Vanishing Gradients", Graph. Models, 66(3), pp. 133-159.
[32] Buchele, S. and Crawford, R., 2003, "Three-Dimensional Halfspace Constructive Solid Geometry Tree Construction from Implicit Boundary Representations", In *Proceedings of the eighth ACM symposium on Solid modeling and applications*, ACM Press, pp. 135-144.
[33] Shapiro, V. and Vossler, D., 1993, "Separation for Boundary to Csg Conversion", ACM Trans. Graph., 12(1), pp. 35-55.
[34] Barthe, L., Dodgson, N., Sabin, M., Wyvill, B., and Gaildrat, V., 2003, "Two-Dimensional Potential Fields for Advanced Implicit Modeling Operators", Computer Graphics Forum, 22(1), pp. 23-33.
[35] Hart, J., 1994, "Distance to an Ellipsoid", Graphics Gems IV, P. Heckbert, eds., Academic Press, Boston, pp. 113-119.
[36] Shin, K.-H., and Dutta, D., 2001, "Constructive Representation of Heterogeneous Objects", Journal of Computing and Information Science in Engineering, 1, pp. 205-217.
[37] Shepard, D., 1968, "A Two-Dimensional Interpolation Function for Irregularly Spaced Data", proceeding of the 23 National Conference, pp. 517-524.
[38] Rvachev, V. L., Sheiko, T. I., Shapiro, V., and Tsukanov, I., 2001, "Transfinite Interpolation Over Implicitly Defined Sets", Computer Aided Geometric Design, 18, pp. 195-220.
[39] Kartasheva, E., Adzhiev, V., Pasko, A., Fryazinov, O., and Gasilov, V., 2003, "Surface and Volume Discretization of Functionally Based Heterogeneous Objects", Journal of Computing and Information Science in Engineering, 3(4), pp. 285-294.